Food Chemistry: X 25 (2025) 102061

Contents lists available at ScienceDirect

Food Chemistry: X

journal homepage: www.sciencedirect.com/journal/food-chemistry-x

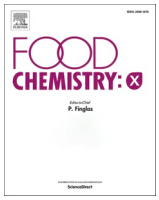

Underlying mechanism of electrospun starch-based nanofiber mats to adsorb the key off-odor compounds of oyster peptides

Linfan Shi [a,b], Zhouru Li [a], Shiqin Qing [a], Zhongyang Ren [a,b], Ping Li [a], Songnan Li [c,**], Wuyin Weng [a,b,*]

[a] College of Ocean Food and Biological Engineering, Jimei University, Xiamen 361021, China
[b] Sericultural & Agri-Food Research Institute Guangdong Academy of Agricultural Sciences, Key Laboratory of Functional Foods, Ministry of Agriculture and Rural Affairs, Guangdong Key Laboratory of Agricultural Products Processing, Guangzhou 510610, China
[c] Joint International Research Laboratory of Agriculture and Agri-Product Safety of the Ministry of Education of China, Institutes of Agricultural Science and Technology Development, Yangzhou University, Yangzhou 225009, Jiangsu, China

ARTICLE INFO

Keywords:
Electrospinning
Octenylsuccinylated starch
Fiber mat
Deodorization
Inclusion complex

ABSTRACT

The solid-phase adsorption principles and fundamental mechanism of isobutyric acid, 1-octen-3-ol, and octanal (three key off-odor compounds of oyster peptides) were explored using electrospun octenyl succinylated starch-pullulan (OSS-PUL) nanofiber mat. The nanofiber mats had selective adsorption behaviors as indicated by the selective adsorption rates of isobutyric acid, 1-octen-3-ol, and octanal, which were 94.96%, 85.03%, and 65.36%. The contents of the II-type inclusion complexes (ICs) formed with the nanofiber mats by the three off-odor compounds mentioned above were significantly different. The mean fiber diameter of the octanal/nanofiber mat IC with the highest content of II-type IC was significantly decreased ($p < 0.05$). In contrast, the isobutyric acid/nanofiber mat IC did not significantly change. The findings suggested that nanofiber mats interacted most strongly with octanal and weakly with isobutyric acid. This study will provide the theoretical foundation for deodorizing aquatic products using electrospun starch-based nanofiber mats.

1. Introduction

Oysters are among the most widely consumed shellfish worldwide due to their high nutritional value and unique flavor. Consumers have been drawn to oyster peptides prepared by enzymatic hydrolysis because of their antioxidant, anti-thrombotic, anti-fatigue, and anti-tumor properties (Chen et al., 2019; Cunha & Pintado, 2022; Luo et al., 2021). However, oyster hydrolysates prepared by this method typically exhibited a grassy, fatty, or fishy off-odor (Liu et al., 2023), which eventually impacted the flavor of the oyster peptides and consumer acceptability. The primary volatile compounds that contributed to this off-odor were aldehydes, alcohols, and acids, primarily produced by oxidation from endogenous protein and lipids during the enzymatic process (Li et al., 2022; Liu et al., 2023). Three important off-odor compounds of oyster peptide were identified by our previous research: isobutyric acid, 1-octen-3-ol, and octanal, with relative odor activity values of 6.22, 51.91 and 43.61, respectively (Li et al., 2022). The off-odor of oyster peptides is caused by the cheesy and acidic flavor of isobutyric acid; the mushroom-like, fishy, and grassy flavor of 1-octen-3-ol; and the grassy and lemon flavor of octanal (Peinado, Miles, & Koutsidis, 2016). According to Liu et al. (2023), 1-octen-3-ol and octanal are primary compounds causing fishy, fatty, and grassy off-odors in Pacific oyster enzymatic hydrolysates. Various techniques have been widely used in the removal of seafood and its by-products, including enzymatic hydrolysis (Sun et al., 2024), yeast fermentation (Shen, Zhang, Mujumdar, & Yang, 2024), chitosan treatment (Liang, Zhang, Fu,

Abbreviations: ANOVA, one-way analysis of variance; ATR-FT-IR, attenuated total reflectance-Fourier transform infrared; DSC, differential scanning calorimetry; HS-GC, headspace-solid gas chromatography; ICs, inclusion complexes; OSS, octenylsuccinated starch; PUL, pullulan; SEM, scanning electron microscopy; T_c, conclusion temperature; T_o, onset temperature; T_p, peak temperature; WCA, water contact angle; XPS, X-ray photoelectron spectroscopy; XRD, X-ray diffraction; ΔH, dissociation enthalpy.

* Corresponding author at: College of Ocean Food and Biological Engineering, Jimei University, Xiamen 361021, China.
** Corresponding author at: Joint International Research Laboratory of Agriculture and Agri-Product Safety of the Ministry of Education of China, Institutes of Agricultural Science and Technology Development, Yangzhou University, Yangzhou 225009, Jiangsu, China
E-mail addresses: lsnyz2020@yzu.edu.cn (S. Li), wwymail@jmu.edu.cn (W. Weng).

https://doi.org/10.1016/j.fochx.2024.102061
Received 26 June 2024; Received in revised form 19 November 2024; Accepted 29 November 2024
Available online 2 December 2024

Zhu, & Mou, 2020), and solid phase adsorption with active clay, zeolite or diatomite (Song et al., 2018). However, the underlying mechanism of solid phase adsorption by electrospun nanofiber mats was limited.

Electrospinning is a method for the production of nanostructured polymer mats. As starch is one of the important polymer sources for electrospinning fiber production, starch-based electrospinning has been extensively studied in terms of raw materials, processes and applications (Cruz et al., 2023; Zhu et al., 2022). Currently, sweet potato starch (Cruz et al., 2023), potato starch (Fonseca et al., 2020) and modified starch such as octenyl succinylated starch (OSS, Li et al., 2022) have been used in the preparation of as-spun nanofiber mats. Regarding the process, dry electrospinning stands out for its environmental friendliness and simplicity (Li, Kong, & Ziegler, 2021). The high porosity and large specific surface area of as-spun nanofiber mats render them highly effective for the adsorption of volatile compounds (Guo, Huang, Xue, & Wang, 2016; Ojstršek et al., 2020). According to Kadam et al. (2018), xylene (173 μg/mg) and formaldehyde (0.07 μg/mg) might be adsorbed by electrospun β-cyclodextrin/polyacrylonitrile mats. According to Shin, Lee, and Ahn (2018), low-density polyethylene and triacetyl-β-cyclodextrin functionalized fiber mats efficiently removed dimethyl sulfide, carbon disulfide, and dimethyl disulfide, with a dimethyl disulfide adsorption rate as high as 90.33%.

Starch is an abundant natural polymer polysaccharide with numerous desirable properties, including safety, renewability, non-toxicity, and biodegradability (Zhao et al., 2024). Since native starch is poorly soluble in water, dimethyl sulfoxide or formic acid is frequently used as an electrospinning solvent (Lancuski, Vasilyev, Putaux, & Zussman, 2015; Zhu et al., 2022). Currently, starch-based electrospinning has been thoroughly studied. However, the use of organic solvents significantly limited the production and application of electrospun starch-based fiber in the food industry. One way to overcome this challenge was using modified starches like OSS to gradually produce starch-based fibers (Li et al., 2021). OSS is a safe food additive with excellent amphiphilic and interfacial properties due to the partial replacement of the hydrophilic hydroxyl groups of native starch by hydrophobic OS groups (Kurdziel, Krolikowska, Labanowska, Pietrzyk, & Michalec, 2020). Furthermore, OSS tended to form molecular entanglements that facilitated fiber formation in an aqueous solution, indicating its potential for electrospinning after dissolution in water (Huang et al., 2024). In our previous research, a “green” electrospinning method was developed for the production of starch-based nanofiber mats with OSS and pullulan (PUL) as raw materials and water as the sole solvent (Li et al., 2022).

The adsorption rules and underlying mechanism between starch-based fiber mats and important off-odor compounds were unclear, despite our demonstration that electrospun OSS-PUL mats could adsorb off-odor compounds of oyster peptide and still exhibited adsorption rates of more than 80% after 25 cycles (Li et al., 2022; Shi et al., 2024). In this study, three important off-odor compounds of oyster peptides including isobutyric acid, 1-octen-3-ol, and octanal, were selected as representatives and further adsorbed in a solid environment using electrospun OSS-PUL fiber mats. The adsorption capacity of these three main off-odor compounds in oyster peptides was determined using differential scanning calorimetry (DSC) and headspace gas chromatography (HS-GC) using electrospun OSS-PUL fiber mats. Scanning electron microscopy (SEM), attenuated total reflectance-Fourier transform infrared (ATR-FTIR) spectroscopy, X-ray diffraction (XRD), water contact angle (WCA) measurement, and X-ray photoelectron spectroscopy (XPS) were used to characterize the structural characteristics of electrospun OSS-PUL fiber mats and their inclusion complexes (ICs). We investigated the underlying mechanism and adsorption principles of electrospun OSS-PUL fiber mats’ in the solid-phase adsorption of three important oyster peptide off-odor compounds. These findings may shed some insight into how electrospun starch-based fiber mats adsorb compounds and reduce the off-odor of aquatic products.

2. Materials and methods

2.1. Materials

OSS (Purity Gum Ultra) was obtained from Ingredion (Shanghai, China) and food-grade PUL was purchased from the Meihua Biotechnology Group Co. Ltd. (Hebei, China). Using an SEM (Phenom-World, Netherlands), their morphologies (Fig. S1) were discovered. We used size-exclusion chromatography and ^{1}H nuclear magnetic resonance to determine the molecular weight (86.59×10^{4} g/mol, Fig. S2) and degree of substitution (0.016, Fig. S3) of the OSS, respectively. Three off-odor compounds were obtained from Macklin Biochemical Co., Ltd. (Shanghai, China): isobutyric acid (99% purity), 1-octen-3-ol (99% purity), and octanal (99% purity). Their physicochemical characteristics and flavor descriptions are listed in Table S1. Furthermore, their mass spectra are displayed in Fig. S4.

2.2. Dope preparation

After dispersing equal amounts of OSS and PUL in deionized water, the mixtures were brought to a boil and constantly stirred for approximately 1 h. Once complete dissolution occurred and the mixtures cooled to room temperature (25 °C), a spinning dope with a concentration of 30% was produced.

2.3. Electrospinning

The electrospinning system (JDF05, Nano Apparatus Technology Co., Ltd., Changsha, China) included a high voltage supply (Dongwen High Voltage Power Supply Co., Tianjin, China), a grounded roller and a syringe pump. The spinning solution was mounted on a syringe pump and filled into a 20 mL syringe. Fibers were created by jetting using a 23-gauge blunt needle with outer and inner diameters of 0.63 and 0.33 mm, respectively, at a solution flow rate of 0.2 mL/h, spinning distance of 11 cm, drum speed of 5 rpm and voltage of about 18 kV (Li et al., 2022).

2.4. Solid-phase adsorption

As-spun fiber mat (0.1 g) and off-odor-compound agents (1 μL) were inserted into a 20 mL headspace, sealed, and heated at 65 °C for 15 mins. After cooling to 25 °C, the fiber mat IC and off-odor compounds were extracted. The following equation was used to calculate the adsorption rate (Q_i):

$$Q_i\ (\%) = (C_0 – C_i)/C_0 \times 100\% \quad (1)$$

Wherein C_0 and C_i are the total compounds with an off-odor before and after adsorption.

2.5. Determination of off-odor compounds

The injector conditions for the HS (HS-10, Shimadzu, Tokyo, Japan) were a thermostat temperature of 70 °C, clamping for one minute, and an injection time of one minute were. The volatile chemicals in the samples were identified using a GC system (GC-2010 Plus, Shimadzu, Tokyo, Japan) equipped with an HP-5 capillary column (30 m × 0.25 mm × 0.25 μm, Agilent Technologies Inc., Santa Clara, CA, USA). Nitrogen was used as the carrier gas for the GC system, with flow rates of 1.5 mL/min for the column, 3 mL/min for the purge gas, 400 mL/min for the air, 40 mL/min for hydrogen, and 30 mL/min for the make-up gas. The heating process was as follows: the initial temperature was 40 °C, increasing to 220 °C at a rate of 20 °C per min (Li et al., 2022). The system had a detector temperature of 300 °C, an inlet temperature of 250 °C, a pressure of 100 kPa, and a split ratio 2:1.

2.6. Characterization of the fiber mats and their ICs

2.6.1. Morphology

A digital camera (Z 30, Nikon, Tokyo, Japan) was used to capture the macro-morphology of the samples (20 mm × 20 mm) in the same orientation. The 10 mm × 10 mm samples were fixed onto an SEM stage, and at 5 kV, the micro-morphology of the samples sprayed with gold film was examined.

2.6.2. Fiber diameter analysis

The fiber diameter distribution of the samples was determined by using Image J software (National Institutes of Health, Bethesda, MD, USA) to analyze their SEM images (20000×) (Shi et al., 2024). A total of 150 points were selected for measurement from each sample, and Origin 19.0 was used to plot the relative frequency distribution.

2.6.3. Pore area analysis

The relative frequency distribution of the pore area was created based on this data using Image J software; the pore area at 250 locations within each sample's 20,000× SEM images was calculated using Origin 18.0 software, as described by Shi, Li, Yang, et al. (2024).

2.6.4. DSC

A DSC (Thermal Advantage Q2000, TA Instrument, New Castle, DE, USA) was used to measure the samples' thermal properties (Shi, Li, Yang, et al., 2024). After adding 1 mg of as-spun fiber mat or IC, weighed using a microbalance, and 3 μL of deionized water, the DSC pan was sealed and equilibrated for 2 h at 25 °C. The assay results for the acquired samples were compared to those obtained from an empty pan subjected to a temperature range of 20 °C to 130 °C at a heating rate of 10 °C/min.

2.6.5. FT-IR spectroscopy

ATR-FTIR spectrometer (Nicolet iS50, Thermo Fisher Scientific Inc., Waltham, MA, USA) was used to measure the samples (Weligama Thuppahige et al., 2023). The FTIR equipment was configured to perform 16 scans at a resolution of 4 cm^{-1} and a wavenumber range of 4000–400 cm^{-1}.

2.6.6. XRD

The crystalline structure of the sample was examined using an XRD system (Ultima-IV, Rigaku, Tokyo, Japan) equipped with Cu-Kα radiation ($\lambda = 0.154$ nm) (Dai et al., 2024). The XRD patterns (ranging from 5°–35° 2θ) were acquired at 40 kV and 30 mA, using a 0.02° step size and 0.5°/min velocity.

2.6.7. Determination of WCA

An SDC-200 instrument (Shengding Precision Instrument Co., Ltd., Dongguan, China) was used to calculate the WCA of the samples (Shi, Li, Zhang, et al., 2024). A slide was covered with a fiber mat, and 1 μL of distilled water was added. The contact angle value was determined where the water droplet made contact with the fiber mat surface using the three-point approach.

2.6.8. XPS

A Thermo Scientific K-Alpha XPS system (Thermo Fisher Scientific Inc., Waltham, MA, USA) was used to examine the surface features of samples (5 mm × 5 mm) (Cui et al., 2023). Al Kα rays with a hv = 1486.6 eV served as the XPS system's excitation source. Narrow and wide spectra were recorded at 50 eV (0.1 eV increments) and 150 eV (1 eV steps). The C_{1s} peak value of 284.8 eV served as the basis for all spectrum adjustments. Software (Advantage 5.948, Thermo Fisher Scientific Inc., Waltham, MA, USA) was used to process the experimental data.

2.7. Statistical analysis

Repeated data ($n \geq 3$) from each experiment was expressed as mean ± standard deviation. Using SPSS software (SPSS, Inc., Chicago, IL, USA), the means were compared using one-way analysis of variance (ANOVA) and Duncan's multiple range test at $p < 0.05$ of significance.

3. Results and discussion

3.1. Adsorption capacity

Using as-spun OSS-PUL fiber mats, three important off-odor compounds of oyster peptides—isobutyric acid, 1-octen-3-ol, and octanal—were selected to study their underlying solid-phase adsorption reaction mechanism. Table 1 illustrates the adsorption capabilities of the as-spun OSS-PUL fiber mats for isobutyric acid, 1-octen-3-ol, and octanal. For isobutyric acid, 1-octen-3-ol, and octanal (*w*/w), their adsorption rates were 94.96 ± 1.28%, 85.03 ± 1.90%, and 65.36 ± 2.45%, respectively, with significant differences observed among them ($p < 0.05$). According to a prior study, 1-octen-3-ol and isobutyric acid were absorbed on as-spun OSS-PUL fiber mats at rates of 58.37% and 100%, respectively, while no significant adsorption efficiency was noted for octanal (Li et al., 2022). The adsorption rates of isobutyric acid and 1-octen-3-ol by the as-spun OSS-PUL fiber mats in this study were broadly consistent with the prior study's findings. The observed increase in the octanal adsorption rate on the as-spun OSS-PUL fiber mats may be attributed to an increased concentration of the monomer adsorption system and the lack of competition from other off-odor oyster peptides (Tefera, Hashisho, Philips, Anderson, & Nichols, 2014; Zhang et al., 2022). The as-spun OSS-PUL fiber mats presented different adsorption rates (65.36%–94.96%) for the three off-odor compounds of oyster peptides, demonstrating their selective adsorption characteristics. The morphology and physicochemical structure of as-spun OSS-PUL fiber mats and ICs were further characterized in this study to better understand the underlying interaction mechanism between the three off-odor compounds of oyster peptides and the fiber mats.

3.2. Morphology and microstructure

Table 1 displays the mean fiber diameter and mean pore area of the as-spun OSS-PUL fiber mats and ICs, whereas Fig. 1 displays their morphology and microstructure. As-spun OSS-PUL fiber mats retained a good morphology and were compatible with the reported results of Li et al. (2022), featuring white, smooth, bead-free, continuous, irregularly orientated, and uniformly distributed nanofibers (Fig. 1A). There were no discernible changes in the macro- and micro-morphology of isobutyric acid/fiber mat IC, 1-octen-3-ol/fiber mat IC, or octanal/fiber mat IC during solid-phase adsorption. Based on these details, the macroscopic and microscopic morphology of as-spun OSS-PUL fiber mats were not affected by the adsorption method for any of the three off-odor compounds of oyster peptides.

The as-spun OSS-PUL fiber mat, 1-octen-3-ol/fiber mat IC, isobutyric acid/fiber mat IC, and octanal/fiber mat IC all exhibited fiber sizes that were normally distributed throughout the 120–260 nm range (Fig. 1B). Their corresponding mean fiber diameters were 185.33 ± 25.30 nm, 184.21 ± 22.14 nm, 184.19 ± 24.63 nm, and 179.53 ± 21.80 nm, respectively (Table 1). Interestingly, the strong interaction between the as-spun OSS-PUL fiber mat and octanal resulted in a significant decrease ($p < 0.05$) in the mean fiber diameter of the octanal/fiber mat IC compared to the original fiber mats. This finding suggested that the fiber diameter of ICs was influenced by the strength of the interaction force between as-spun OSS-PUL fiber mats and octanal, affecting the fiber diameter of ICs. With mean pore areas of $(3.39 \pm 1.29) \times 10^5$ nm^2, $(3.30 \pm 1.42) \times 10^5$ nm^2, $(3.20 \pm 1.22) \times 10^5$ nm^2, and $(3.25 \pm 1.62) \times 10^5$ nm^2 (Table 1), respectively, the pore areas of as-spun OSS-PUL fiber mats, isobutyric acid/fiber mat IC, 1-octen-3-ol/fiber mat IC, and

Table 1
Adsorption, microstructure and thermal properties of the as-spun OSS-PUL nanofiber mats and their ICs.

Sample	Adsorption rate (%)	Microstructure		Thermal properties			
		Mean fiber diameter (nm)	Mean pore area ($\times 10^5$ nm^2)	T_o (°C)	T_p (°C)	T_c(°C)	$\triangle H$ (J/g)
Nanofiber mat	–	185.33 ± 25.30^a	3.39 ± 1.29^a	–	–	–	–
Isobutyric acid/ nanofiber mat IC	94.96 ± 1.28^a	184.21 ± 22.14^{ab}	3.30 ± 1.42^a	133.15 ± 4.12^a	133.48 ± 3.91^a	135.90 ± 1.42^a	0.67 ± 0.01^b
1-Octen-3-ol/ nanofiber mat IC	85.03 ± 1.90^b	184.19 ± 24.63^{ab}	3.20 ± 1.22^a	128.44 ± 0.37^a	128.87 ± 0.35^a	136.72 ± 0.36^a	0.93 ± 0.02^a
Octanal/ nanofiber mat IC	65.36 ± 2.45^c	179.53 ± 21.80^b	3.25 ± 1.62^a	131.00 ± 0.54^a	131.43 ± 0.23^a	135.52 ± 2.01^a	0.69 ± 0.05^b

Samples with different superscript letters in a column are significantly different ($p < 0.05$).

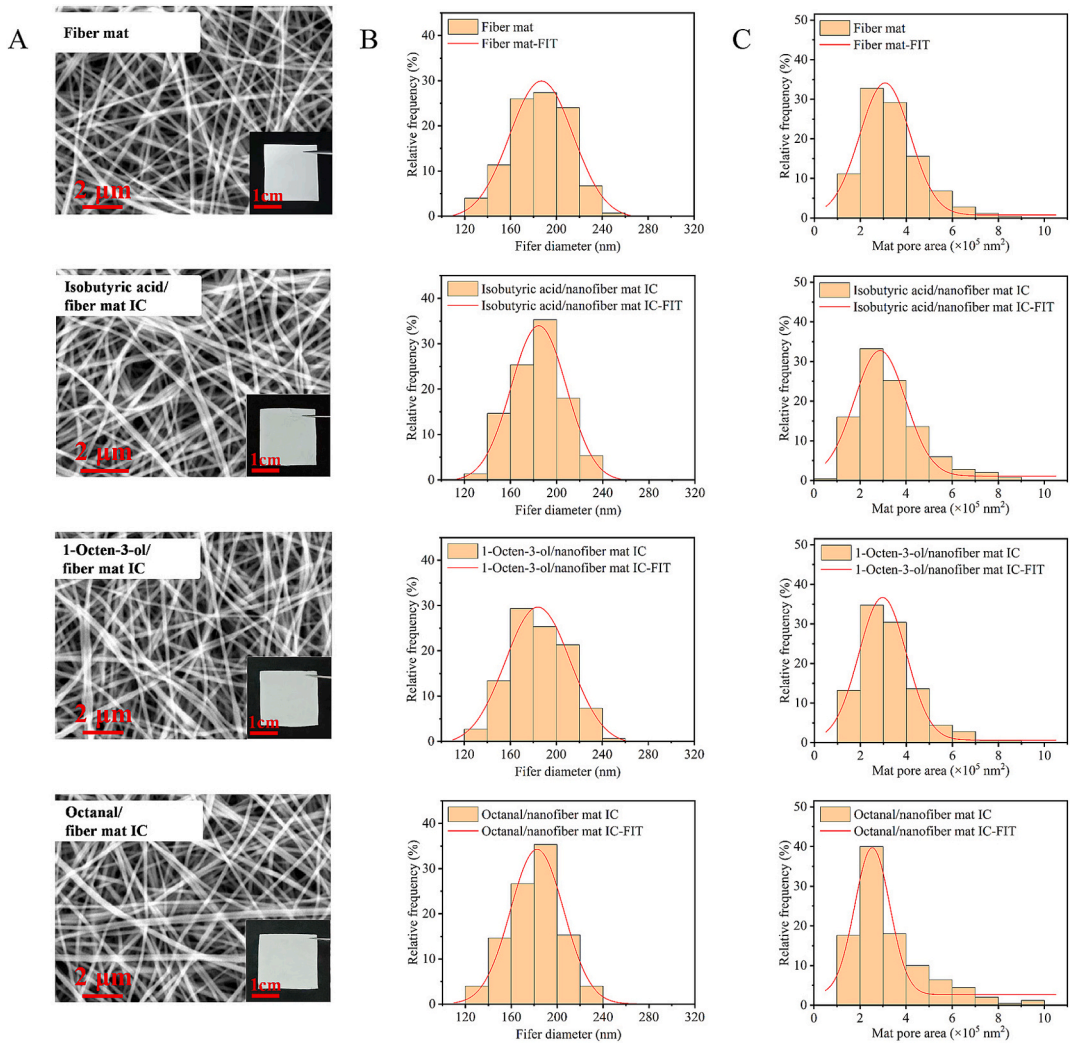

Fig. 1. Morphology (A), fiber diameter distribution (B) and pore area distribution (C) of the as-spun OSS-PUL nanofiber mats and their ICs.

octanal/fiber mat IC also closely conformed to the normal distribution (Fig. 1C). The fact that none of them were significantly different from each other suggests that the adsorption of these three off-odor compounds of oyster peptides by as-spun OSS-PUL fiber mats did not affect their pore size.

3.3. Characterization

3.3.1. Thermal properties

The DSC thermograms of the samples are shown in Fig. 2A, and Table 1 displays the thermal characteristics related to their structure and composition, including dissociation enthalpy (ΔH), onset temperature (T_o), peak temperature (T_p), conclusion temperature (T_c), and so on. The number of guest molecules in IC is reflected in the ΔH. The temperature at which IC dissociates is represented by T_p, which divides them into II-type ($T_p > 100$ °C) and I-type ($T_p < 100$ °C) groups (Fan et al., 2022). II-type ICs with higher T_p values have better thermal stability and a more ordered structure (Guo, Shi, & Kong, 2023). Fig. 2A shows no adsorption peak in the 60 °C–140 °C range for the as-spun OSS-PUL nanofiber mat, consistent with previous work (Shi, Li, Yang, et al., 2024). As demonstrated by the clear endothermic peak at T_p of 133.48 ± 3.91 °C, 128.87 ± 0.35 °C, and 131.43 ± 0.23 °C (Fig. 2A) for isobutyric acid/nanofiber

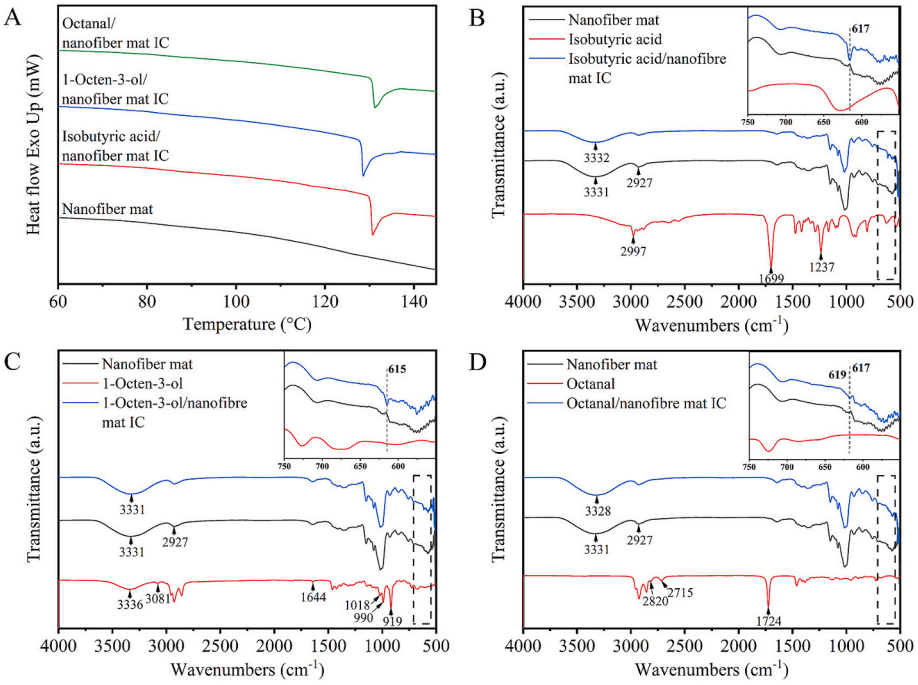

Fig. 2. DSC thermograms (A) and FT-IR spectra (B–D) of the as-spun OSS-PUL nanofiber mats and their ICs.

mat IC, 1-octen-3-ol/nanofiber mat IC, and octanal/nanofiber mat IC, respectively, these three oyster peptide off-odor compounds could form II-type ICs with as-spun OSS-PUL nanofiber mats. The results showed that the as-spun OSS-PUL mat ICs with the top three oyster peptide off-odor compounds exhibited exceptional thermal stability (Zhou & Kong, 2023). Of these, 1-octen-3-ol/nanofiber mat IC had the highest guest molecule content ($\Delta H = 0.93 \pm 0.02$ J/g), with a significant difference ($p < 0.05$) compared to octanal/nanofiber mat IC ($\Delta H = 0.69 \pm 0.05$ J/g) and isobutyric acid/nanofiber mat IC ($\Delta H = 0.67 \pm 0.01$ J/g). It was noteworthy that the GC data, which did not entirely accord with the DSC results, showed that the adsorption rates of three off-odor compounds of oyster peptides by as-spun OSS-PUL nanofiber mats were isobutyric acid, 1-octen-3-ol, and octanal in decreasing order. The reason for the partial desorption of isobutyric acid and low ΔH of the isobutyric acid/nanofiber mat IC could be attributed to the poor interaction between as-spun OSS-PUL nanofiber mats and isobutyric acid, which prevented the formation of stable ICs.

3.3.2. *Infrared spectroscopy*

FTIR spectroscopy was used to study the complexing properties and adsorption mechanism of as-spun OSS-PUL mats with off-odor compounds of the oyster peptide. The findings are shown in Fig. 2B–D. The stretching of O—H, C═O, and C—O in isobutyric acid was identified as the cause of the vibrations at 2976 cm^{-1}, 1699 cm^{-1}, and 1237 cm^{-1}, respectively. The O—H stretching vibration was represented by the broad absorption band of 1-octen-3-ol at 3336 cm^{-1}; the C—H stretching vibration, C═C stretching vibration, and C—H out-of-plane bending vibration in the olefin was indicated by the bands at 3081 cm^{-1}, 1644 cm^{-1}, 990 cm^{-1}, and 919 cm^{-1}; the band represented the C—O stretching vibration at 1018 cm^{-1}. The bispectral bands of 2820 cm^{-1} and 2715 cm^{-1} represented the Fermi resonance band of C—H in the aldehyde group, the primary distinctive peak of the octanal at 1724 cm^{-1} was caused by the C═O stretching (Luo et al., 2021). The as-spun OSS-PUL nanofiber mats' maxima at 2927 cm^{-1} and 3331 cm^{-1}, respectively, belonged to the C—H and O—H stretching vibrations (Gao, Sui, Liu, Cui, & Abd El-Aty, 2021). The stretching of C—O, C—C, and C-O-H and the bending of the C-O-H were the causes of the peaks in the 1000–1200 cm^{-1} region (Warren, Gidley, & Flanagan, 2016). The FTIR spectra of the three ICs were essentially comparable to the as-spun OSS-PUL mats, as shown in Fig. 2B–D. This suggested that three oyster peptide off-odor compounds were adsorbed within the as-spun OSS-PUL mats. The peaks of 1-octen-3-ol and isobutyric acid/nanofiber mat IC increased at 617 cm^{-1}, and the peak of octanal/nanofiber mat IC at 617 cm^{-1} displayed a little red shift. According to the results of the DSC, it was discovered that three oyster peptide off-odor compounds formed ICs with as-spun OSS-PUL nanofiber mats.

3.3.3. *Crystalline structure*

Fig. 3A displays the findings of the XRD. The as-spun OSS-PUL nanofiber mat exhibited broad diffraction peak at 7.6° and 21.0° (2θ), respectively, indicating the presence of an amorphous structure. Zhang et al. (2024) prepared starch mats using wheat, potato, and cassava starches though the heated dissolution method and casting method, respectively, and obtained that all of them showed an amorphous structure in XRD analysis. Thermoplastic stretching during heating was one of the reasons for disrupting the crystalline regions of starch. During thermoplastic stretching, the crystalline areas of starch disrupted by temperature and shear force (Yang et al., 2023). In addition, H_2O molecules break the hydrogen bonds in the crystalline areas of OSS/PUL, hindering the recrystallization process and resulting in an amorphous structure of the as-spun OSS-PUL nanofiber mat (Lv et al., 2024). The diffraction peaks of 1-octen-3-ol/nanofiber mat IC, octanal/nanofiber mat IC, and isobutyric acid/nanofiber mat IC did not significantly change when compared to as-spun OSS-PUL nanofiber mats. This suggested that the adsorption of three off-odor compounds of oyster peptides does not alter the crystalline structure of as-spun OSS-PUL nanofiber mats. According to the results of a previous study, it was assumed that the IC production resulted from the physical adsorption process (Li et al., 2022). The slight enhancement at 7° 2θ correlated with the strength of starch-guest molecule interactions (Sun et al., 2023). This suggested that as-spun OSS-PUL mats interacted with three oyster peptide off-odor compounds, which was consistent with the DSC and FTIR results of this study.

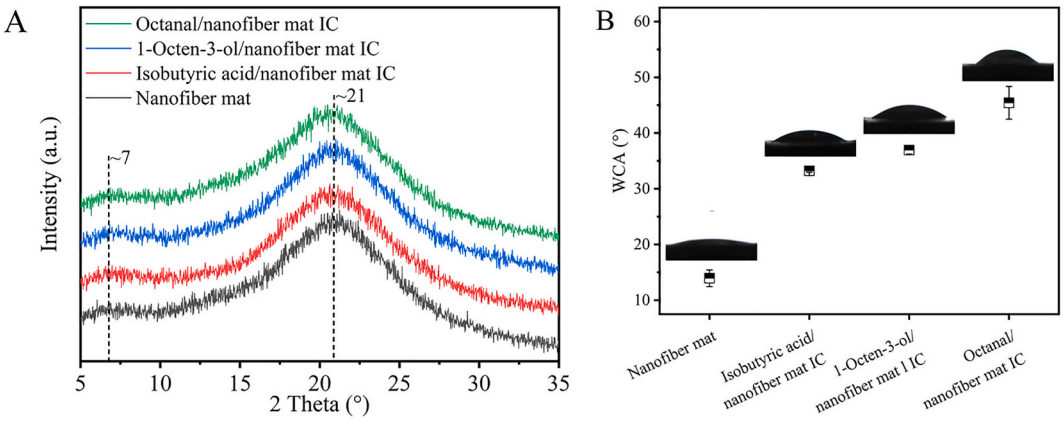

Fig. 3. XRD spectra (A) and WCA (B) of the as-spun OSS-PUL nanofiber mats and their ICs.

3.4. Surface wettability

Fig. 3B shows the WCA of ICs and as-spun OSS-PUL mats. In contrast to the previously published finding of 29.01° (Shi, Li, Yang, et al., 2024), the WCA of the as-spun OSS-PUL nanofiber mat was 13.59 ± 1.50°. Deionized water was used as the sole solvent for manufacturing the as-spun OSS-PUL nanofiber mat; however, as the water evaporated during storage, the WCA of the mat increased. The WCAs for 1-octen-3-ol/nanofiber mat IC, octanal/nanofiber mat IC, and isobutyric acid/nanofiber mat IC were 33.20 ± 0.22°, 36.94 ± 0.71°, and 45.43 ± 2.94°, respectively. As a result of isobutyric acid's strong water solubility (49,180 mg/L, Api et al., 2020) and its weakest interaction with as-spun OSS-PUL nanofiber mat, the results showed that isobutyric acid/nanofiber mat IC was the least hydrophobic. The results of the DSC indicated that the weak contact caused the isobutyric acid/nanofiber mat IC to be unstable and the isobutyric acid to be desirable. Because these two oyster peptide off-odor compounds were less soluble (1,836 mg/L and 560 mg/L), their hydrophobicity was higher in the 1-octen-3-ol/nanofiber mat IC and octanal/nanofiber mat IC due to their lengthy hydrophobic carbon chains.

3.5. Surface characteristics

Three elements were presented in the as-spun OSS-PUL nanofiber mat: C, O, and Na (Fig. S5), with C_{1s} and O_{1s} having greater peak intensities. The C_{1s} narrow spectrum contained O-C=O (288.7 eV), C=O/O-C-O (287.7 eV), C—O (286.4 eV), and C-C/C=C (284.8 eV) peaks (Fig. 4A) (Sifuentes-Nieves et al., 2020). The O_{1s} narrow spectrum was divided into three peaks, including O-C=O (533.5 eV), C-O-C (532.8 eV), and C-O/C=O (531.4 eV) (Fig. 4B) (Wang, Liu, Chen, Mo, & Zhang, 2022; Yu, Yu, Dong, & Xia, 2022).

As-spun OSS-PUL nanofiber mats exhibited rich contributions of C—O (54.06%), C-C/C=C (27.13%), C=O/O-C-O (15.82%), and O-C=O (2.99%) in their C_{1s} spectra (Table 2). The relative peak area of the O-C=O on the surface of the isobutyric acid/nanofiber mat IC was significantly increased, originating from the carboxyl group (O-C=O) of isobutyric acid. Both the 1-octen-3-ol/nanofiber mat IC and the octanal/nanofiber mat IC showed considerably higher C-C/C=C values. According to these findings, 1-octen-3-ol and octanal's lengthy hydrophobic carbon chains may have enhanced the hydrophobicity of respective ICs when combined with as-spun OSS-PUL nanofiber mats. A correlation coefficient (r) of 0.78 was found between the values of C-C/C=C and WCA. From the O_{1s} spectra, O-C=O, C-O-C, and C-O/C=O values were 10.07%, 83.81%, and 6.13%, respectively (Table 2). Notably, for the isobutyric acid/nanofiber mat IC and octanal/nanofiber mat IC, the values of O-C=O and C-O/C=O increased. Consistent with the previous findings, the elevated values of O-C=O and C-O/C=O for isobutyric acid/nanofiber mat IC were attributed to the accumulation of carboxyl groups (-COOH) during IC formation. The enhanced C-O/C=O value for the octanal/nanofiber mat IC was sourced from the aldehyde group (-CHO) of octanal, while the synthesis of acetals between the hydroxyl and -CHO groups on the as-spun OSS-PUL nanofiber mat surface may have contributed to the higher O-C=O value (Wang et al., 2016). Finally, in agreement with DSC and GC data, XPS results verified that isobutyric acid, 1-octen-3-ol, and octanal successfully formed ICs with as-spun OSS-PUL nanofiber mats.

3.6. Adsorption mechanism

The as-spun OSS-PUL mats that had the highest adsorption capacity (94.96 ± 1.28%) were able to adsorb isobutyric acid, which was in line with the preference of as-spun OSS-PUL mats for adsorption in acids found in a previous study (Li et al., 2022). According to the HS-GC data, a new peak with the highest peak strength emerged in the FTIR spectrum in the isobutyric acid/nanofiber mat IC. DSC analysis demonstrated that an as-spun OSS-PUL nanofiber mat with good heat stability formed II-type ICs with isobutyric acid. On the other hand, the DSC thermogram of the isobutyric acid/nanofiber mat IC revealed the lowest ΔH, suggesting that some of the ICs formed from as-spun OSS-PUL nanofiber mats containing isobutyric acid were unstable. The partial dissociation of unstable isobutyric acid molecules from isobutyric acid/nanofiber mat IC after interacting with water is likely caused by the excellent hydrophilicity of as-spun OSS-PUL nanofiber mats (WCA of 13.59 ± 1.50°) (Zhou & Kong, 2023). Furthermore, there was no discernible change in the macrostructure or microstructure (fiber diameter and pore area) of the isobutyric acid/nanofiber mat IC. This finding suggested that the interaction between the as-spun OSS-PUL nanofiber mat and isobutyric acid was weak, making the mat susceptible to desorption. The adsorption and desorption mechanism of isobutyric acid by as-spun OSS-PUL mats was notably reversible. According to our previous research, after 25 cycles, the adsorption rate of isobutyric acid by the regenerated OSS-PUL nanofiber mats remained at 100%, indicating that the process was unaffected by the number of regenerations (Shi, Li, Zhang, et al., 2024).

As-spun OSS-PUL nanofiber mat adsorbed 65.36 ± 2.45% of the octanal, and the FTIR spectra showed no new peaks for the octanal/nanofiber mat IC, except for a slightly redshifted peak at 617 cm^{-1}. Nonetheless, DSC demonstrated that II-type ICs, with ΔH of 0.69 ± 0.05 J/g, were successfully formed between as-spun OSS-PUL nanofiber mats and octanal; this was comparable to the ΔH of 0.67 ± 0.01 J/g seen for isobutyric acid/nanofiber mat IC. These results revealed that despite the low rate of octanal adsorption by the nanofiber mat, the IC exhibited strong contact, was challenging to desorb, and had good thermal stability. Furthermore, the microstructure of the octanal/nanofiber mat IC demonstrated a significant reduction in mean fiber diameter ($p < 0.05$), suggesting a strong interaction between them. As proven by XPS, the

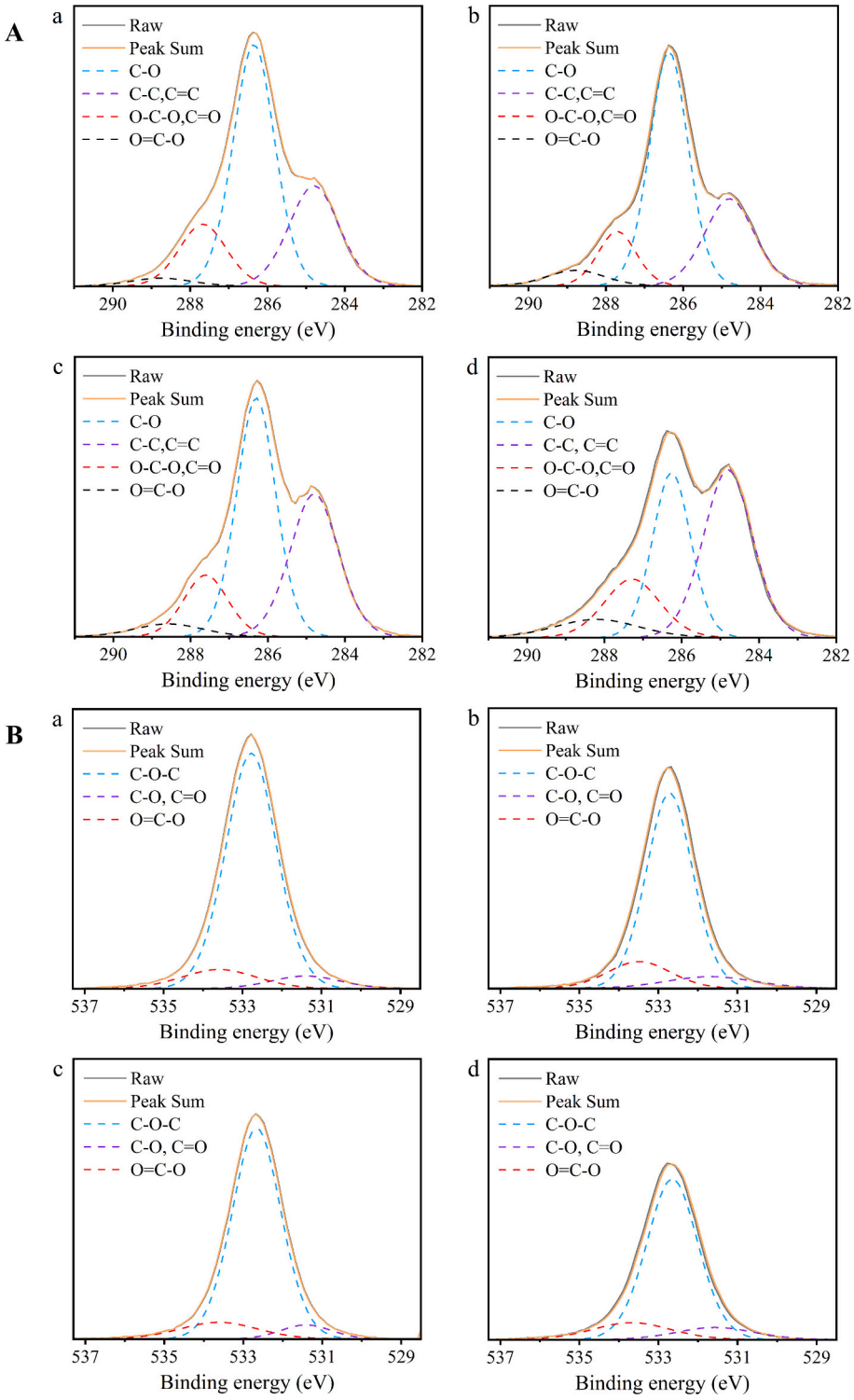

Fig. 4. C_{1s} (A) and O_{1s} (B) spectra of the as-spun OSS-PUL nanofiber mats (a), isobutyric acid/nanofiber mat IC (b), 1-octen-3-ol/nanofiber mat IC (c) and octanal/nanofiber mat IC (d).

aldehyde group of octanal may have condensed with the hydroxyl group of as-spun OSS-PUL nanofiber mats. These findings indicated that as-spun OSS-PUL nanofiber mats and octanal successfully formed ICs and that their interaction was more substantial than the isobutyric acid/nanofiber mat IC. The intensity of the interaction may also influence the as-spun OSS-PUL mat's adsorption rate on the two off-odor compounds of oyster peptide (Yoon, Kim, & Kim, 1998).

The as-spun OSS-PUL mat's adsorption rate for 1-octen-3-ol was 85.03 ± 1.90%, which fell between the adsorption rates of the two previously described off-odor compounds of oyster peptide. DSC, FTIR spectroscopy, and XPS were used to confirm the synthesis of the 1-octen-3-ol/nanofiber mat IC. Despite their microstructure (fiber diameter) not changing considerably, 1-octen-3-ol/nanofiber mat IC was found to exhibit a significantly greater enthalpy (ΔH = 0.93 ± 0.02 J/g) compared to the other two ICs ($p < 0.05$). These results showed that the interaction between as-spun OSS-PUL nanofiber mats and 1-octen-3-ol

Table 2
Relative content of groups on the surface of the as-spun OSS-PUL nanofiber mats and their ICs.

Sample	Relative content (%)						
	C_{1s}				O_{1s}		
	C-O	C-C, C=C	O-C-O, C=O	O=C-O	C-O-C	C-O, C=O	O=C-O
Nanofiber mat	54.06	27.13	15.82	2.99	83.81	6.13	10.07
Isobutyric acid/ nanofiber mat IC	55.21	26.54	12.74	5.51	76.51	9.04	14.46
1-Octen-3-ol/ nanofiber mat IC	47.05	34.77	13.71	4.48	83.51	5.86	10.62
Octanal/ nanofiber mat IC	32.52	42.65	16.91	7.92	78.17	9.12	12.71

was stronger than that between as-spun OSS-PUL nanofiber mats and isobutyric acid, but weaker than that between as-spun OSS-PUL nanofiber mats and octanal.

As-spun OSS-PUL mat demonstrated selective adsorption capacity, and the order of the adsorption rate was isobutyric acid (94.96%) > 1-octen-3-ol (85.03%) > octanal (65.36%). Both DSC and FTIR results confirmed that octanal, 1-octen-3-ol and isobutyric acid formed II-type ICs with as-spun OSS-PUL nanofiber mats, and the interaction intensities of these compounds with the mats decreased in order. Physical adsorption was used in the as-spun OSS-PUL nanofiber mat complexation method with off-odor compounds. Hydrophobic, hydrostatic, and hydrogen bonding interactions could all occur (Liang et al., 2023).

4. Conclusions

The adsorption rates of isobutyric acid, 1-octen-3-ol, and octanal on as-spun OSS-PUL nanofiber mat were determined to be 94.96 ± 1.28%, 85.03 ± 1.90%, and 65.36 ± 2.45%, respectively, using HS-GC, DSC, FTIR spectroscopy and XPS in this study. It was presumed that there was selectivity in the adsorption of these compounds and that the formation process of the three off-odor compounds/as-spun OSS-PUL nanofiber mat ICs was physical adsorption. The macrostructure and microstructure of the three ICs showed no significant changes; however, the octanal/nanofiber mat IC's fiber diameter was significantly decreased, which was attributed to the strong interaction between octanal and electrospun OSS-PUL nanofiber mat. Additionally, acetals may have been formed between the hydroxyl group of the electrospun OSS-PUL nanofiber mat and the aldehyde group of the octanal. It is noteworthy that the isobutyric acid/nanofiber mat IC had the lowest concentration (ΔH = 0.67 ± 0.01 J/g) of the guest molecule according to the DSC results. It was hypothesized that the three off-odor compounds interacted with the electrospun OSS-PUL nanofiber mat in the following decreasing order: octanal, 1-octen-3-ol, and isobutyric acid. The molecular structure and hydrophobicity of off-odor compounds may be related to the hydrophobicity of the ICs, which followed octanal/nanofiber mat IC, 1-octen-3-ol/nanofiber mat IC, and isobutyric acid/nanofiber mat IC in decreasing order of hydrophobicity. This study added to the theoretical foundation for the potential applications of electrospun starch-based nanofiber mats and the high-value utilization and flavor improvement of aquatic products by demonstrating how electrospun OSS-PUL nanofiber mats can form ICs with off-odor compounds. The binding sites and interaction forces between electrospun OSS-PUL nanofiber mats and key off-odor compounds of oyster peptides remain unclear, which could be further clarified by adsorption kinetics and molecular simulation techniques in the future work.

CRediT authorship contribution statement

Linfan Shi: Writing – review & editing, Writing – original draft, Investigation, Data curation. **Zhouru Li:** Writing – original draft, Investigation, Data curation. **Shiqin Qing:** Writing – review & editing, Data curation. **Zhongyang Ren:** Writing – review & editing. **Ping Li:** Writing – review & editing. **Songnan Li:** Writing – review & editing, Funding acquisition, Conceptualization. **Wuyin Weng:** Writing – review & editing, Funding acquisition, Conceptualization.

Declaration of competing interest

The authors declare that they have no known competing financial interests or personal relationships that could have appeared to influence the work reported in this paper.

Acknowledgments

The authors thank the financial support received from National Natural Science Foundation of China (32302141/32272266), and Natural Science Foundation of Fujian Province (2024J09042). Dr. Songnan Li gratefully acknowledges the financial support from the Natural Science Foundation of Jiangsu Province (BK20220585), China Postdoctoral Science Foundation (2022M712692) and the "QingLan" Talent Support Program of Yangzhou University.

Appendix A. Supplementary data

Supplementary data to this article can be found online at https://doi.org/10.1016/j.fochx.2024.102061.

Data availability

The authors do not have permission to share data.

References

Api, A. M., Belsito, D., Biserta, S., Botelho, D., Bruze, M., Burton, G. A., Jr., … Tsang, S. (2020). RIFM fragrance ingredient safety assessment, isobutyric acid, CAS registry number 79-31-2. *Food and Chemical Toxicology, 144*, Article 111673. https://doi.org/10.1016/j.fct.2020.111673

Chen, H., Cheng, S., Fan, F., Tu, M., Xu, Z., & Du, M. (2019). Identification and molecular mechanism of antithrombotic peptides from oyster proteins released in simulated gastro-intestinal digestion. *Food & Function, 10*(9), 5426–5435. https://doi.org/10.1039/c9fo01433k

Cruz, E. P. D., Jansen, E. T., Fonseca, L. M., Hackbart, H., Siebeneichler, T. J., Pires, J. B., … Dias, A. R. G. (2023). Red onion skin extract rich in flavonoids encapsulated in ultrafine fibers of sweet potato starch by electrospinning. *Food Chemistry, 406*, Article 134954. https://doi.org/10.1016/j.foodchem.2022.134954

Cui, J., Niu, X., Zhang, D., Ma, J., Zhu, X., Zheng, X., Lin, Z., & Fu, M. (2023). The novel chitosan-amphoteric starch dual flocculants for enhanced removal of *Microcystis aeruginosa* and algal organic matter. *Carbohydrate Polymers, 304*, Article 120474. https://doi.org/10.1016/j.carbpol.2022.120474

Cunha, S. A., & Pintado, M. E. (2022). Bioactive peptides derived from marine sources: Biological and functional properties. *Trends in Food Science & Technology, 119*, 348–370. https://doi.org/10.1016/j.tifs.2021.08.017

Dai, Y., Ren, Z., Li, P., Zhang, Y., Weng, W., & Shi, L. (2024). Selective adsorption of volatile compounds of oyster peptides by V-type starch for effective deodorization. *Food Hydrocolloids, 147*, Article 109295. https://doi.org/10.1016/j.foodhyd.2023.109295

Fan, H., Chen, Z., Xu, L., Wen, Y., Li, H., Wang, J., & Sun, B. (2022). Both alkyl chain length and V-amylose structure affect the structural and digestive stability of amylose-alkylresorcinols inclusion complexes. *Carbohydrate Polymers, 292*, Article 119567. https://doi.org/10.1016/j.carbpol.2022.119567

Fonseca, L. M., Radünz, M., Dos Santos Hackbart, H. C., da Silva, F. T., Camargo, T. M., Bruni, G. P., … Dias, A. R. G. (2020). Electrospun potato starch nanofibers for thyme essential oil encapsulation: Antioxidant activity and thermal resistance. *Journal of the Science of Food and Agriculture, 100*(11), 4263–4271. https://doi.org/10.1002/jsfa.10468

Gao, W., Sui, J., Liu, P., Cui, B., & Abd El-Aty, A. M. (2021). Synthetic mechanism of octenyl succinic anhydride modified corn starch based on shells separation pretreatment. *International Journal of Biological Macromolecules, 172*, 483–489. https://doi.org/10.1016/j.ijbiomac.2021.01.082

Guo, J., Shi, L., & Kong, L. (2023). Structure-digestibility relationship of starch inclusion complex with salicylic acid. *Carbohydrate Polymers, 299*, Article 120147. https://doi.org/10.1016/j.carbpol.2022.120147

Guo, Z., Huang, J., Xue, Z., & Wang, X. (2016). Electrospun graphene oxide/carbon composite nanofibers with well-developed mesoporous structure and their adsorption performance for benzene and butanone. *Chemical Engineering Journal, 306*, 99–106. https://doi.org/10.1016/j.cej.2016.07.048

Huang, X., Teng, Z., Xie, F., Wang, G., Li, Y., Liu, X., & Li, S. (2024). Loading of cinnamon essential oil into electrospun octenylsuccinylated starch-pullulan nanofiber mats: Electrospinnability evaluation, structural characterization, and antibacterial potential. *Food Hydrocolloids, 148*, Article 109426. https://doi.org/10.1016/j.foodhyd.2023.109426

Kadam, V., Truong, Y. B., Easton, C. D., Mukherjee, S., Wang, L., Padhye, R., & Kyratzis, I. L. (2018). Electrospun polyacrylonitrile/β-cyclodextrin composite membranes for simultaneous air filtration and adsorption of volatile organic compounds. *ACS Applied Nano Materials, 1*(8), 4268–4277. https://doi.org/10.1021/acsanm.8b01056

Kurdziel, M., Krolikowska, K., Labanowska, M., Pietrzyk, S., & Michalec, M. (2020). The effect of thermal and irradiation treatments on structural and physicochemical properties of octenyl succinate maize starches. *Food Chemistry, 330*, Article 127242. https://doi.org/10.1016/j.foodchem.2020.127242

Lancuski, A., Vasilyev, G., Putaux, J. L., & Zussman, E. (2015). Rheological properties and electrospinnability of high-amylose starch in formic acid. *Biomacromolecules, 16*(8), 2529–2536. https://doi.org/10.1021/acs.biomac.5b00817

Li, S., Kong, L., & Ziegler, G. R. (2021). Electrospinning of octenylsuccinylated starch-pullulan nanofibers from aqueous dispersions. *Carbohydrate Polymers, 258*, Article 116933. https://doi.org/10.1016/j.carbpol.2020.116933

Li, Z., Weng, W., Ren, Z., Zhang, Y., Li, S., & Shi, L. (2022). Electrospun octenylsuccinylated starch-pullulan nanofiber mats: Adsorption for the odor of oyster peptides and structural characterization. *Food Hydrocolloids, 133*, Article 107992. https://doi.org/10.1016/j.foodhyd.2022.107992

Liang, S., Du, J., Hong, Y., Cheng, L., Gu, Z., Li, Z., & Li, C. (2023). Octenyl succinate anhydride debranched starch-based nanocarriers for curcumin with improved stability and antioxidant activity. *Food Hydrocolloids, 135*, Article 108118. https://doi.org/10.1016/j.foodhyd.2022.108118

Liang, S., Zhang, T., Fu, C., Zhu, C., & Mou, H. (2020). Partially degraded chitosan-based flocculation to achieve effective deodorization of oyster (*Crassostrea gigas*) hydrolysates. *Carbohydrate Polymers, 234*, Article 115948. https://doi.org/10.1016/j.carbpol.2020.115948

Liu, L., Zhao, Y., Lu, S., Liu, Y., Xu, X., & Zeng, M. (2023). Metabolomics investigation on the volatile and non-volatile composition in enzymatic hydrolysates of Pacific oyster (*Crassostrea gigas*). *Food Chemistry: X, 17*, Article 100569. https://doi.org/10.1016/j.fochx.2023.100569

Luo, X., Hou, Y., Xie, X., Qin, Z., Ji, H., & Chen, J. (2021). Role of water on ozonation of cinnamaldehyde to benzaldehyde under ca $(OH)_2$ catalysis: A combined in situ DRIFTS and DFT study. *Applied Surface Science, 569*, Article 151071. https://doi.org/10.1016/j.apsusc.2021.151071

Luo, X., Liu, W., Zhong, H., Yan, Y., Feng, F., & Zhao, M. (2021). Synergistic effect of combined oyster peptide and ginseng extracts on anti-exercise-fatigue and promotion of sexual interest activity in male ICR mice. *Journal of Functional Foods, 86*, Article 104700. https://doi.org/10.1016/j.jff.2021.104700

Lv, H., Xu, H., Xu, E., Jin, Z., Zhao, H., Yuan, C., Zhao, M., Wu, Z., He, D., & Cui, B. (2024). Improving structural and functional properties of starch-catechin-based green nanofiber mats for active food packaging by electrospinning and crosslinking techniques. *International Journal of Biological Macromolecules, 267*, Article 131460. https://doi.org/10.1016/j.ijbiomac.2024.131460

Ojstršek, A., Fakin, D., Hribernik, S., Fakin, T., Bračič, M., & Kurečič, M. (2020). Electrospun nanofibrous composites from cellulose acetate/ultra-high silica zeolites and their potential for VOC adsorption from air. *Carbohydrate Polymers, 236*, Article 116071. https://doi.org/10.1016/j.carbpol.2020.116071

Peinado, I., Miles, W., & Koutsidis, G. (2016). Odour characteristics of seafood flavour formulations produced with fish by-products incorporating EPA, DHA and fish oil. *Food Chemistry, 212*, 612–619. https://doi.org/10.1016/j.foodchem.2016.06.023

Shen, J., Zhang, M., Mujumdar, A. S., & Yang, C. (2024). Synergistic pre-deodorization effect of lysozyme and yeast extracts with high-voltage electrostatic field on crab meatballs. *Food Bioscience, 59*, Article 104033. https://doi.org/10.1016/j.fbio.2024.104033

Shi, L., Li, Z., Yang, Z., Ren, Z., Zhang, Y., & Weng, W. (2024). Adsorption characteristics of V-type starch for off-odors of sea cucumber intestinal peptides in solid-phase environment. *Food Chemistry, 433*, Article 137171. https://doi.org/10.1016/j.foodchem.2023.137171

Shi, L., Li, Z., Zhang, Y., Ren, Z., Zhang, Y., Li, S., & Weng, W. (2024). Electrospun starch-based nanofiber mats for odor adsorption of oyster peptides: Recyclability and structural characterization. *Food Hydrocolloids, 147*, Article 109408. https://doi.org/10.1016/j.foodhyd.2023.109408

Shin, J., Lee, E. J., & Ahn, D. U. (2018). Electrospinning of tri-acetyl-β-cyclodextrin (TA-β-CD) functionalized low-density polyethylene to minimize sulfur odor volatile compounds. *Food Packaging and Shelf Life, 18*, 107–114. https://doi.org/10.1016/j.fpsl.2018.10.005

Sifuentes-Nieves, I., Flores-Silva, P. C., Gallardo-Vega, C., Hernandez-Hernandez, E., Neira-Velazquez, G., Mendez-Montealvo, G., & Velazquez, G. (2020). Films made from plasma-modified corn starch: Chemical, mechanical and barrier properties. *Carbohydrate Polymers, 237*, Article 116103. https://doi.org/10.1016/j.carbpol.2020.116103

Song, G., Zhang, M., Peng, X., Yu, X., Dai, Z., & Shen, Q. (2018). Effect of deodorization method on the chemical and nutritional properties of fish oil during refining. *LWT-Food Science and Technology, 96*, 560–567. https://doi.org/10.1016/j.lwt.2018.06.004

Sun, S., Hong, Y., Gu, Z., Cheng, L., Ban, X., Li, Z., & Li, C. (2023). Different starch varieties influence the complexing state and digestibility of the resulting starch-lipid complexes. *Food Hydrocolloids, 141*, Article 108679. https://doi.org/10.1016/j.foodhyd.2023.108679

Sun, X., Liu, X., Yang, W., Feng, A., Sun, T., Jiang, Q., & Xie, W. (2024). Establishment of intermittent ultrasound-complex enzyme deodorization technology for tilapia based on GC-IMS and HS-SPME-GC/MS analysis. *Food Bioscience, 61*, Article 104806. https://doi.org/10.1016/j.fbio.2024.104806

Tefera, D. T., Hashisho, Z., Philips, J. H., Anderson, J. E., & Nichols, M. (2014). Modeling competitive adsorption of mixtures of volatile organic compounds in a fixed-bed of beaded activated carbon. *Environmental Science & Technology, 48*(9), 5108–5117. https://doi.org/10.1021/es404667f

Wang, H., Liu, R., Chen, Q., Mo, Y., & Zhang, Y. (2022). Biochar-supported starch/chitosan-stabilized nano-iron sulfide composites for the removal of lead ions and nitrogen from aqueous solutions. *Bioresource Technology, 347*, Article 126700. https://doi.org/10.1016/j.biortech.2022.126700

Wang, W., Jin, X., Zhu, Y., Zhu, C., Yang, J., Wang, H., & Lin, T. (2016). Effect of vapor-phase glutaraldehyde crosslinking on electrospun starch fibers. *Carbohydrate Polymers, 140*, 356–361. https://doi.org/10.1016/j.carbpol.2015.12.061

Warren, F. J., Gidley, M. J., & Flanagan, B. M. (2016). Infrared spectroscopy as a tool to characterise starch ordered structure–a joint FTIR-ATR, NMR, XRD and DSC study. *Carbohydrate Polymers, 139*, 35–42. https://doi.org/10.1016/j.carbpol.2015.11.066

Weligama Thuppahige, V. T., Moghaddam, L., Welsh, Z. G., Wang, T., Xiao, H., & Karim, A. (2023). Extraction and characterisation of starch from cassava (*Manihot esculenta*) agro-industrial wastes. *LWT - Food Science and Technology, 182*, Article 114787. https://doi.org/10.1016/j.lwt.2023.114787

Yang, N., Gao, W., Zou, F., Tao, H., Guo, L., Cui, B., … Wu, Z. (2023). The relationship between molecular structure and film-forming properties of thermoplastic starches from different botanical sources. *International Journal of Biological Macromolecules, 230*, Article 123114. https://doi.org/10.1016/j.ijbiomac.2022.123114

Yoon, J. Y., Kim, J. H., & Kim, W. S. (1998). Interpretation of protein adsorption phenomena onto functional microspheres. *Colloids and Surfaces B: Biointerfaces, 12*(1), 15–22. https://doi.org/10.1016/S0927-7765(98)00045-9

Yu, Z., Yu, D., Dong, J., & Xia, W. (2022). Ultrasound-reinforced encapsulation of proanthocyanidin by chitosan-chondroitin sulfate nanosystem. *Food Hydrocolloids, 132*, Article 107872. https://doi.org/10.1016/j.foodhyd.2022.107872

Zhang, L., Zhao, J., Li, F., Jiao, X., Yang, B., & Li, Q. (2024). Effects of amylose and amylopectin fine structure on the thermal, mechanical and hydrophobic properties of starch films. *International Journal of Biological Macromolecules, 282*, Article 137018. https://doi.org/10.1016/j.ijbiomac.2024.137018

Zhang, W., Li, G., Yin, H., Zhao, K., Zhao, H., & An, T. (2022). Adsorption and desorption mechanism of aromatic VOCs onto porous carbon adsorbents for emission control and resource recovery: Recent progress and challenges. *Environmental Science: Nano, 9*(1), 81–104. https://doi.org/10.1039/D1EN00929J

Zhao, Y., Tu, D., Wang, D., Xu, J., Zhuang, W., Wu, F., & Tian, Y. (2024). Structural and property changes of starch derivatives under microwave field: A review. *International Journal of Biological Macromolecules, 256*, Article 128465. https://doi.org/10.1016/j.ijbiomac.2023.128465

Zhou, J., & Kong, L. (2023). Complexation with pre-formed "empty" V-type starch for encapsulation of aroma compounds. *Food Science and Human Wellness, 12*(2), 488–494. https://doi.org/10.1016/j.fshw.2022.07.050

Zhu, W., Zhang, D., Liu, X., Ma, T., He, J., Dong, Q., Din, Z., Zhou, J., Chen, L., Hu, Z., & Cai, J. (2022). Improving the hydrophobicity and mechanical properties of starch nanofibrous films by electrospinning and cross-linking for food packaging applications. *LWT - Food Science and Technology, 169*, Article 114005. https://doi.org/10.1016/j.lwt.2022.114005